T. DOMAŃSKI*, A. BOKOTA**

NUMERICAL MODELS OF HARDENING PHENOMENA OF TOOLS STEEL BASE ON THE TTT AND CCT DIAGRAMS

MODELE NUMERYCZNE ZJAWISK HARTOWANIA STALI NARZĘDZIOWEJ OPARTE NA WYKRESACH CTPi ORAZ CTPc

In work the presented numerical models of tool steel hardening processes take into account thermal phenomena, phase transformations and mechanical phenomena. Numerical algorithm of thermal phenomena was based on the Finite Elements Methods in Galerkin formula of the heat transfer equations. In the model of phase transformations, in simulations heating process, isothermal or continuous heating (CHT) was applied, whereas in cooling process isothermal or continuous cooling (TTT, CCT) of the steel at issue. The phase fraction transformed (austenite) during heating and fractions of ferrite, pearlite or bainite are determined by Johnson-Mehl-Avrami formulas. The nescent fraction of martensite is determined by Koistinen and Marburger formula or modified Koistinen and Marburger formula. In the model of mechanical phenomena, apart from thermal, plastic and structural strain, also transformations plasticity was taken into account. The stress and strain fields are obtained using the solution of the Finite Elements Method of the equilibrium equation in rate form. The thermophysical constants occurring in constitutive relation depend on temperature and phase composite. For determination of plastic strain the Huber-Misses condition with isotropic strengthening was applied whereas for determination of transformation plasticity a modified Leblond model was used. In order to evaluate the quality and usefulness of the presented models a numerical analysis of temperature field, phase fraction, stress and strain associated hardening process of a fang lathe of cone shaped made of tool steel was carried out.

Keywords: Quenching, phase transformations, stresses, numerical simulation, tool steel

Prezentowane w pracy modele numeryczne procesów hartowania stali narzędziowej uwzględniają zjawiska cieplne, przemiany fazowe oraz zjawiska mechaniczne. Algorytm numeryczny zjawisk cieplnych oparto na rozwiązaniu metodą elementów skończonych w sformułowaniu Galerkina równania przewodzenia ciepła. W modelu przemian fazowych korzysta się, w symulacji procesów nagrzewania, z wykresów izotermicznego lub ciągłego nagrzewania (CTPa), natomiast w procesach chłodzenia, z wykresów izotermicznego lub ciągłego chłodzenia (CTPi, CTPc) rozważanej stali. Ułamek fazy przemienionej (austenit) podczas nagrzewania oraz ułamki ferrytu, perlitu lub bainitu wyznacza się formułami Johnsona-Mehla i Avramiego. Ułamek powstającego martenzytu wyznacza się wzorem Koistinena i Marburgera lub zmodyfikowanym wzorem Koistinena i Marburgera. W modelu zjawisk mechanicznych uwzględniono oprócz odkształceń termicznych, plastycznych i strukturalnych – również odkształcenia transformacyjne. Pola naprężeń i odkształceń uzyskuje się z rozwiązania metodą elementów skończonych równań równowagi w formie prędkościowej. Stałe termofizyczne występujące w związkach konstytutywnych uzależniono od temperatury i składu fazowego. Do wyznaczania odkształceń plastycznych wykorzystano warunek Hubera-Misesa ze wzmocnieniem izotropowym, natomiast do wyznaczania odkształceń transformacyjnych zastosowano zmodyfikowany model Leblonda. W celu oceny jakości i przydatności prezentowanych modeli dokonano analizy numerycznej pól temperatury, udziałów fazowych, naprężeń i odkształceń towarzyszących procesowi hartowania kła tokarki ze stali narzędziowej.

1. Introduction

Thermal treatment including hardening is a complex technological process aiming to obtain high hardness, high abrasion resistance, high durability of the elements hardened as well as suitable initial structure to be used in the subsequent thermal treatment processes as a result of which the optimum mechanical properties of the elements are received. Product of the martensite transformation is primary structure of the steel undergoing hardening.

Today an intense development of numerical methods supporting designing or improvement of already existing technological processes are observed. The technologies mentioned above include also steel thermal processing comprising hardening. Efforts involving thermal process-

* CZESTOCHOWA UNIVERSITY OF TECHNOLOGY, INSTITUTE OF MECHANICS AND MACHINE DESIGN, 42-200 CZĘSTOCHOWA, 73 DĄBROWSKIEGO STR., POLAND

** CZESTOCHOWA UNIVERSITY OF TECHNOLOGY, INSTITUTE OF COMPUTER AND INFORMATION SCIENCES, 42-200 CZĘSTOCHOWA, 73 DĄBROWSKIEGO STR., POLAND

ing numerical models aim to encompass an increasing number of input parameters of such a process [1-4].

Predicting of final properties of the element undergoing hardening is possible after determination of the type and features of the microstructure to be created, as well as of instantaneous and residual stresses accompa-nying such technology of product quality improvement. For this to be achieved, it is necessary to take into account, first of all, thermal phenomena, phase transformations and mechanical phenomena in the numerical model [2,5-9] (Fig. 1).
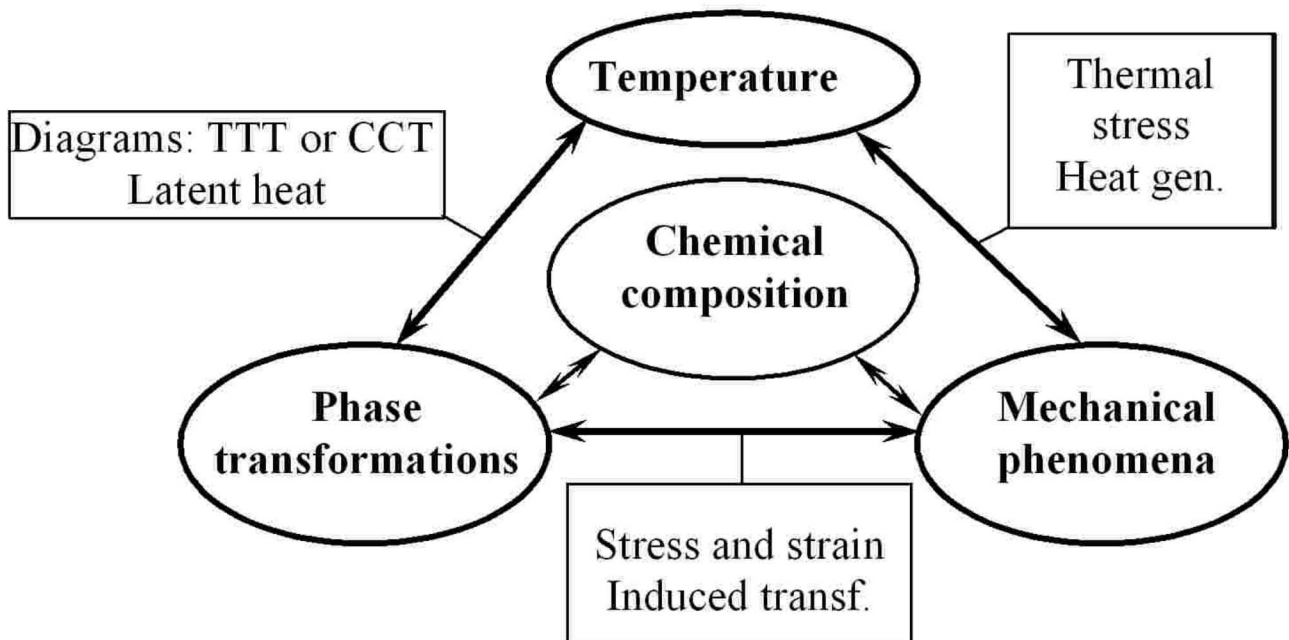

Fig. 1. Scheme of correlation of the hardening phenomena

As a consequence of analyzing of the thermal processing results many mathematical and numerical models were obtained. A basic element of almost all studies regarding transformations of austenite into ferrite, pearlite and bainite is the Avrami equation with respect of the TTT diagram-based models and the general Kolmogorov Johnson-Mehl-Avrami equation with respect to the models using classical nucleation theory [2,4,9,10]. The Koistinen and Marburger's equation is, on the other hand, fundamental equation enabling prediction of the kinetics of the martensite transformation [2-5]. The results of the numerical simulations of the phenomena mentioned above are dependent on the precision in calculation of the instantaneous temperature and solid-state phase kinetics, the latter significantly affecting the instantaneous and residual stresses. Therefore accuracy of the solid-state phase transformations model for each steel grade is very important here. In the study the TTT [1,2,5] and CCT diagram-based models are proposed [5,12].

Phase transformations numerical models exploiting isothermal heating and cooling curves can be applied with respect to several carbon steel grades if the isothermal heating and cooling curves are adequately moved.

However, the values of the curve move should be confirmed by the results of experimental research conducted for this specific or a similar steel grade [1,11,13]. Application of TTT diagrams facilitates parallel calculations and thus it is easier to take the heat of the phase transformations into account in the numerical algorithm [2,4]. On the other hand, CCT diagrams enable more precise determination of fractions and kinetics of the phases depending of the cooling rate [3-5,14].

Numerical simulations of steel thermal processing must be referred to in the transformation strains models [2,4,15]. This phenomenon causes metal irregular plastic flow which is observed during solid-state phase transformations especially during the decomposition of austenite into martensite. Literature presents two separate transformation strains mechanisms, one proposed by Greenwood and Johnson and another one – by Magee [11,16,17]. The Greenwood–Johnson model assumes that transformation plasticity are microplasticity occurring at the weaker austenite phase caused by the difference of specific volume between the phases. In the Magee interpretation (for the martensite transformation) it is a result of a change of the orientation of the newly-created martensite plates caused by external loading. Priorities of these

mechanisms depend on the material and transformation type. The Greenwood–Johnson model prevails in diffusion transformations, but also in the transforamatins of bainite and martensite where the specific volume differs between the phases.

A modified Leblond's model was applied in the study to evaluate the transformation plasticity [17]. Literature mentions other models of evaluation of transformation strains [2,5,16,18]. Netherthless, the Leblond model (based upon the Greenwood–Johnson mechanism) comprises all transformations and is the most popular model applied by researchers dealing with thermal process modeling.

Finite Element Method is the method most frequently used to implement numerical algorithms. This method enables to easily include in the analysis both non-linearity and non-homogeneity of the material thermally processed and therefore in the proposed models both heat conduction equation and equilibrium equations are solved using the Finite Element Method [1,2,19].

Accuracy of the proposed tool steel hardening methods was proved by comparing the results of numerical simulations and experimental research results presented in the studies [7].

2. Phase transformations

In the model of phase transformations take advantage of diagrams of isothermal heating (CHT) and cooling (TTT) and diagrams of continuous heating (CHT) and cooling (CCT) [7,14].

In both case the phase fractions transformed during continuous heating (austenite) is calculated using the Johnson-Mehl and Avrami formula or modified Koistinen and Marburger formula (in relations on rate of heating) [2,3,5]:

$$\underline{\eta}_A(T,t) = 1 - \exp(-b\left(t_s, t_f\right)(t\,(T))^{n\left(t_s, t_f\right)}) \qquad (1)$$

$$\underline{\eta}_A(T,t) = 1 - \exp\left(-\frac{\ln(\eta_s)}{T_{sA} - T_{fA}}(T_{sA} - T)\right), \ \dot{T} \geqslant 100\,K/s \qquad (2)$$

where: $\underline{\eta}_A$ is austenite initial fraction nescent in heating process, T_{sA} is temperature of initial phase in austenite, T_{fA} – is final temperature this phase.

The coefficient $b(t_s, t_f)$ and $n(t_s, t_f)$ are obtain with (1) next assumption of initial fraction (η_s=0.01) and final fraction (η_f=0.99) and calculation are by formula:

$$n\left(t_s, t_f\right) = \frac{\ln(\ln(0.01)/\ln(0.99))}{\ln\left(t_f/t_s\right)}, \ \ b\left(t_s, t_f\right) = \frac{-\ln(0.99)}{(t_s)^n} \qquad (3)$$

Pearlite and bainite fraction (in the model of phase transformations upper and lower bainite is not distinguish) are determine by Johnson-Mehl and Avrami formula. Was used with TTT diagrams apply the formula:

$$\eta_i(T,t) = \left(\underline{\eta}_A - \sum_{j,\,j\neq i} \eta_j\right)\left(1 - \exp\left(-b(T)t^{n(T)}\right)\right) \qquad (4)$$

Take advantage of graph CCT, phase fraction ($\eta_{(.)}$) calculate by formula:

$$\eta_i(T,t) = \beta\left(1 - \exp\left(-b\left(t(T)\right)^n\right)\right) \qquad (5)$$

The nascent fraction of martensite is calculated using the Koistinen and Marburger formula [2,4,5].

$$\eta_M(T) = \beta\left(1 - \exp\left(-c\left(M_s - T\right)\right)\right), \ \ c = \frac{-\ln(0.01)}{M_s - M_f} \qquad (6)$$

or modified Koistinen and Marburger formula [3,4,7]:

$$\eta_M(T) = \beta\left(1 - \exp\left(-\left(\frac{M_s - T}{M_s - M_f}\right)^m\right)\right) \qquad (7)$$

where

$$\beta = \eta_{(.)}^{\%}\underline{\eta}_A \ \text{ for } \ \underline{\eta}_A \geqslant \eta_{(.)}^{\%} \ \text{ and } \ \beta = \underline{\eta}_A \ \text{ for } \ \underline{\eta}_A < \eta_{(.)}^{\%} \qquad (8)$$

$\eta_{(.)}^{\%}$ is the maximum phase fraction for the established of the cooling rate, estimated on the base of the continuous cooling graph, m is the constant chosen by means of experiment. For considered steel determine, that $m = 3.3$ if the start temperature of martensite transformations is equal M_s=493 K, and end this transformations is in temperature M_f=173 K [14].

The choice of suitable model can by dependent on kinds of lead hardening simulations. It can by parallel simulation of thermal phenomena, phase transformations and mechanical phenomena (Fig. 2), or series block simulations – thermal block, phase transformations, and than mechanical phenomena block [3].
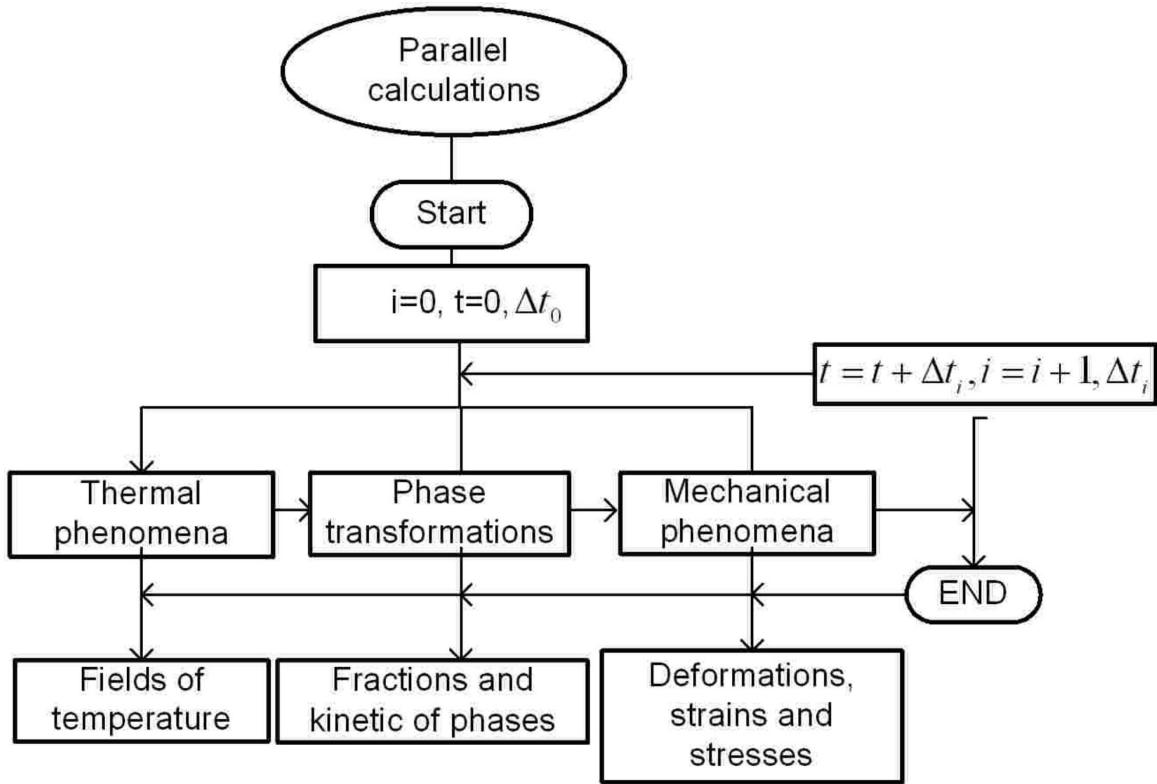
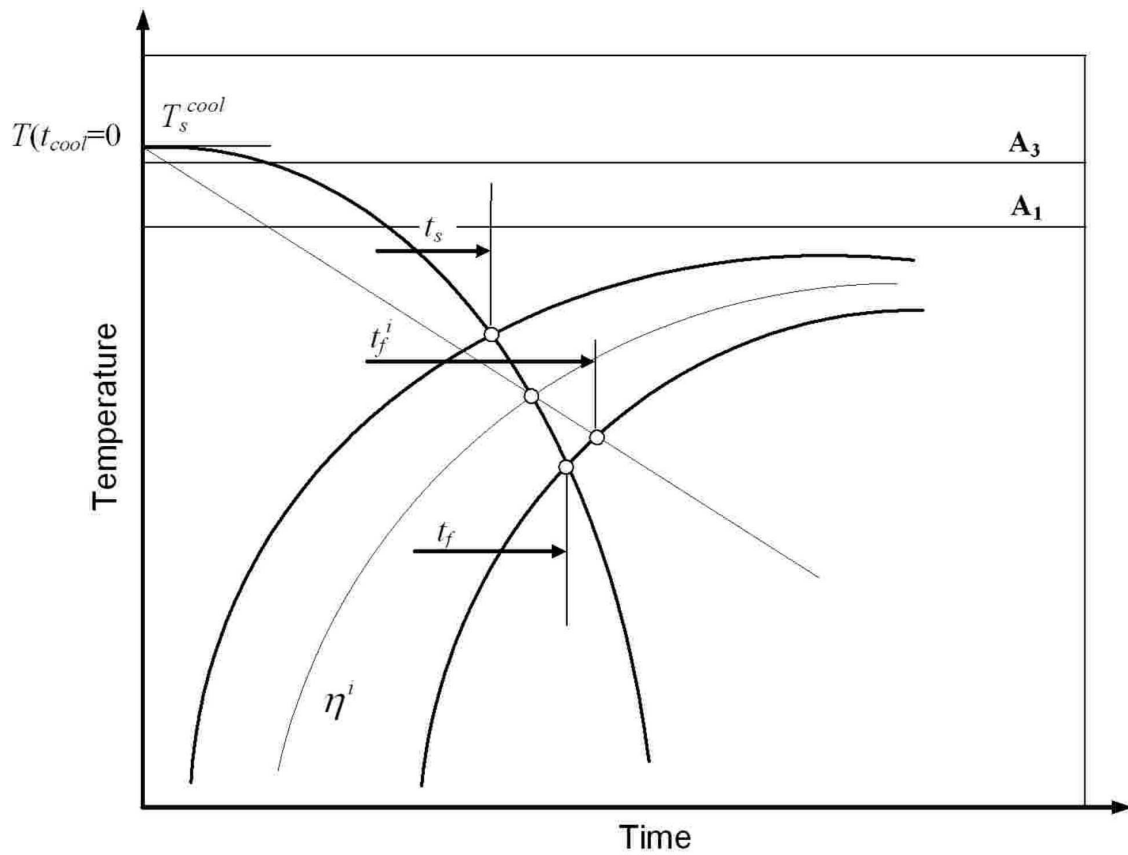Fig. 2. Diagram of parallel hardening simulation

Fig. 3. Determination of time t_f in the parallel simulation (curve CCT, cooling)

Models using diagrams of isothermal heating and cooling can be applied both with respect to parallel and block sequential simulation since the transformations starting and ending times are determined at the crossing of the starting and ending curves of the transformations carried out at a fixed temperature [2,4].

Models using continuous heating and cooling diagrams can be directly applied only in a block sequential simulation. In this case transformation starting and ending times are determined at the crossing of the starting and ending curves of the transformations and the heating or cooling temperature curves. In the parallel simulation model the transformation starting time is directly determined at the crossing of the transformations starting curve and heating or cooling temperature curves whereas the transformation ending time can be established using the technique of temperature curve approximation within the expected range of the transformation (Fig. 3).

It must be emphasised that using isothermal cooling diagrams to calculate phase fractions in the process of continuous cooling requires application of a suitable technique for calculating of the transformations time [2,4]. Transition from time t to $t + \Delta t$ for cooling case was schematically presented in the Fig. 4.

It was accepted that the transformation starts at t_1 at the temperature T_1. By approximation of the cooling curve with a stepped curve in the range of time $\Delta t_1 = t_2 - t_1$ (Fig. 4) a constant temperature of T_1 is maintained. Using the formula (2.4) a volume fraction of the transformation structural element η_1 for the time $t = t_2$. At t_2 temperature rises to the level of T_2 and therefore the temperature T_2 is achieved by moving along the structural component participation line (η_1). The time t_2^*
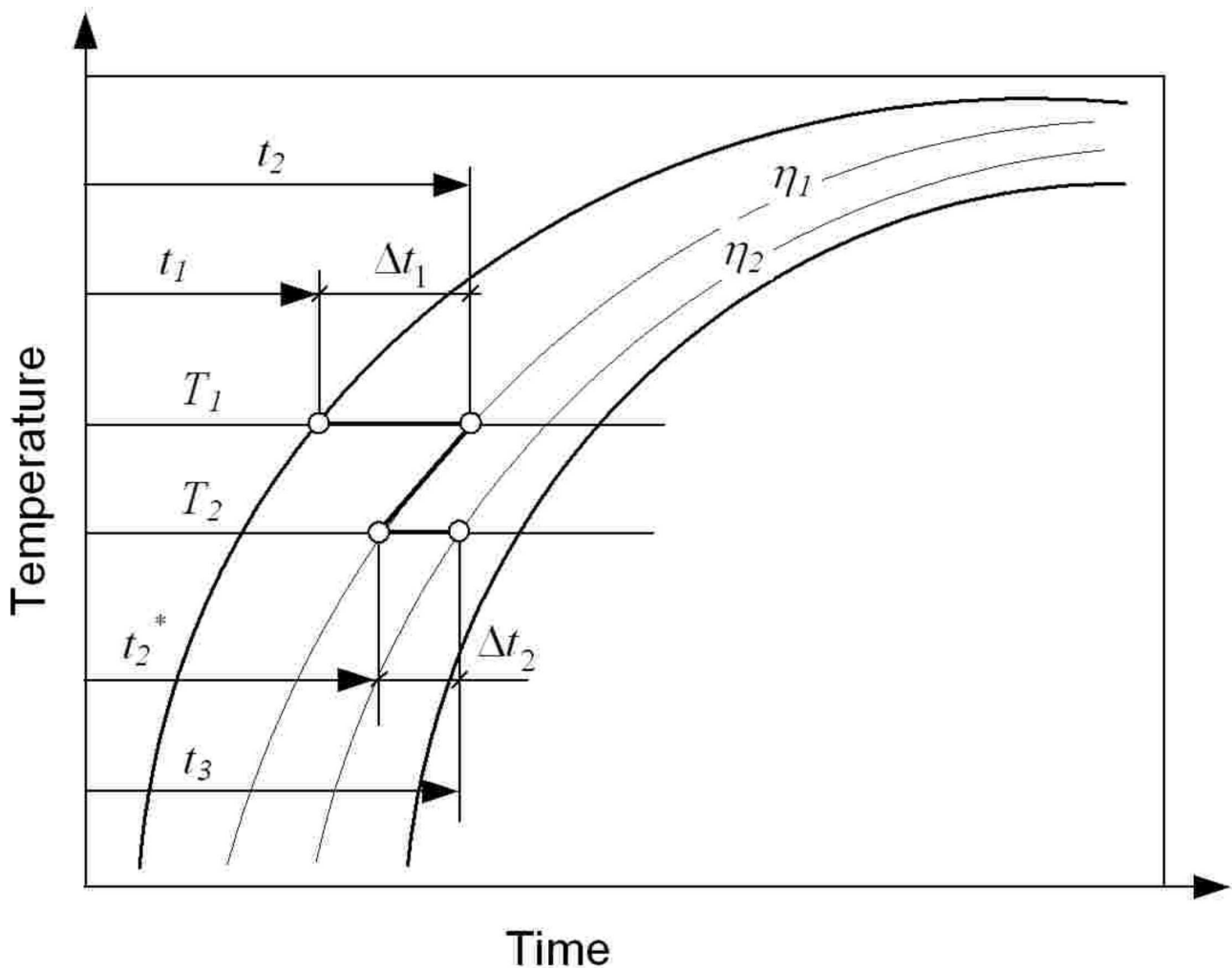

Fig. 4. Illustration of calculation of the transformation time (cooling)

required for the transformation η_1 at the temperature T_2 is calculated using the formula obtained from the transformation (1), to which the temperature T_2 is substituted. As a result the t_2^* formula is obtained:

$$t_2^* = \left(\frac{-\ln(l - \eta_1)}{b(T_2)} \right)^{\frac{1}{n(T_2)}} \qquad (9)$$

The increase $\Delta t_2 = t_3 - t_2$ is added to t_2^* and the volume fraction η_2 is calculated for the time $\tau_2 = t_2^* + \Delta t_2$. Such a technique of calculation of the transformation time involving application of isothermal parts allows using isothermal diagrams to determine fractions of the phases in the continuous cooling process [2,4].

Increases of the isotropic deformation caused by changes of the temperature and phase transformation in the heating and cooling processes are calculated using the following relations:

– heating

$$d\varepsilon^{Tph} = \sum_{\alpha=1}^{\alpha=5} \alpha_\alpha \eta_\alpha dT - \varepsilon_A^{ph} d\eta_A \qquad (10)$$

– cooling

$$d\varepsilon^{Tph} = \sum_{\alpha=1}^{\alpha=5} \alpha_\alpha \eta_\alpha dT + \sum_{\beta=2}^{\beta=5} \varepsilon_\beta^{ph} d\eta_\beta \qquad (11)$$

where: $\alpha_A = \alpha_A(T)$, are coefficients of thermal expansion of: austenite, bainite, ferrite, martensite and pearlite, respectively, ε_A^{ph} is the isotropic deformation accompanying transformation of the input structure into austenite, whereas $\gamma_B = \gamma_B(T)$ are isotropic deformations from phase transformation of: austenite into bainite, ferrite, martensite, or of austenite into pearlite, respectively. These values are usually adopted on the basis of experimental research conducted on a heat cycle simulator [7].

The methods for calculation of the fractions of the phases created referred to above were used for carbon tool steel represented by C80U steel. TTT and CCT diagrams for this steel grade are presented in the Figures 5, 6 and 7.
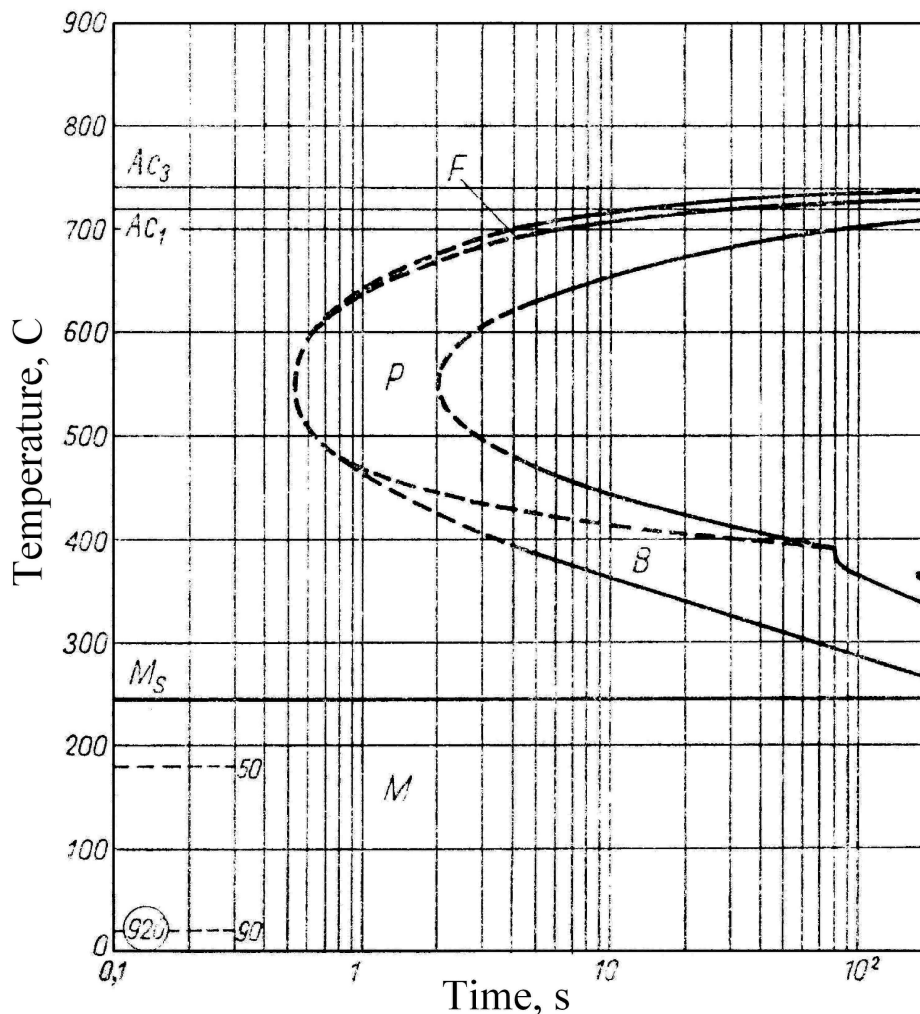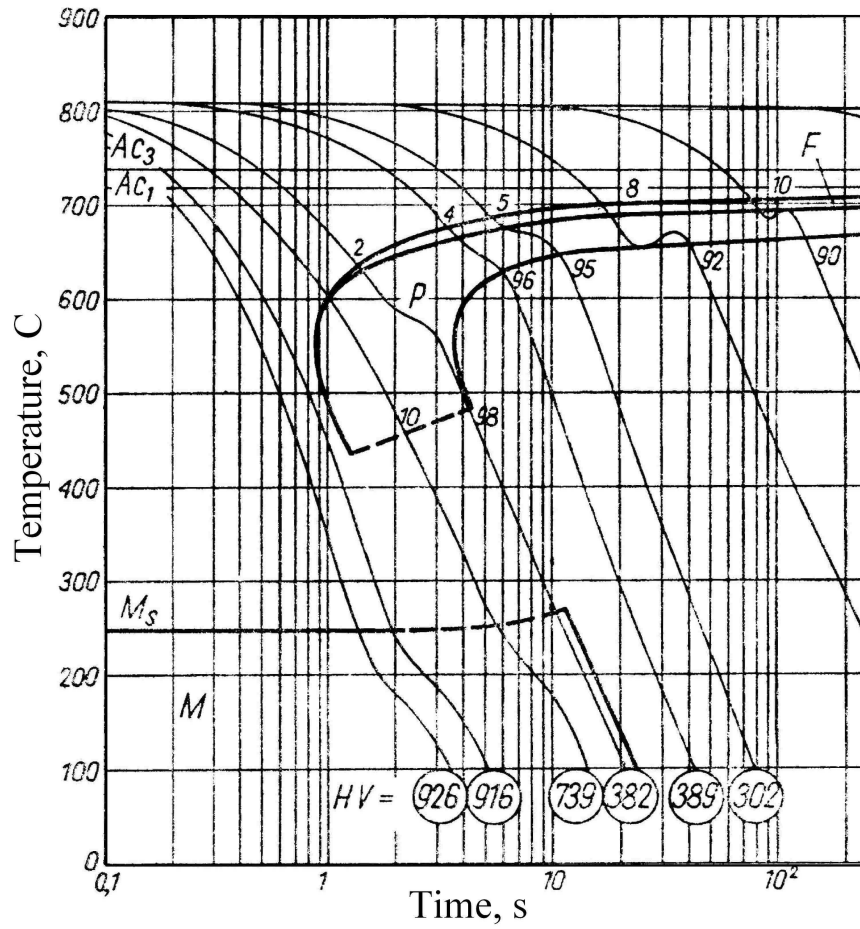

Fig. 5. Diagram TTT for steel C80U [14]

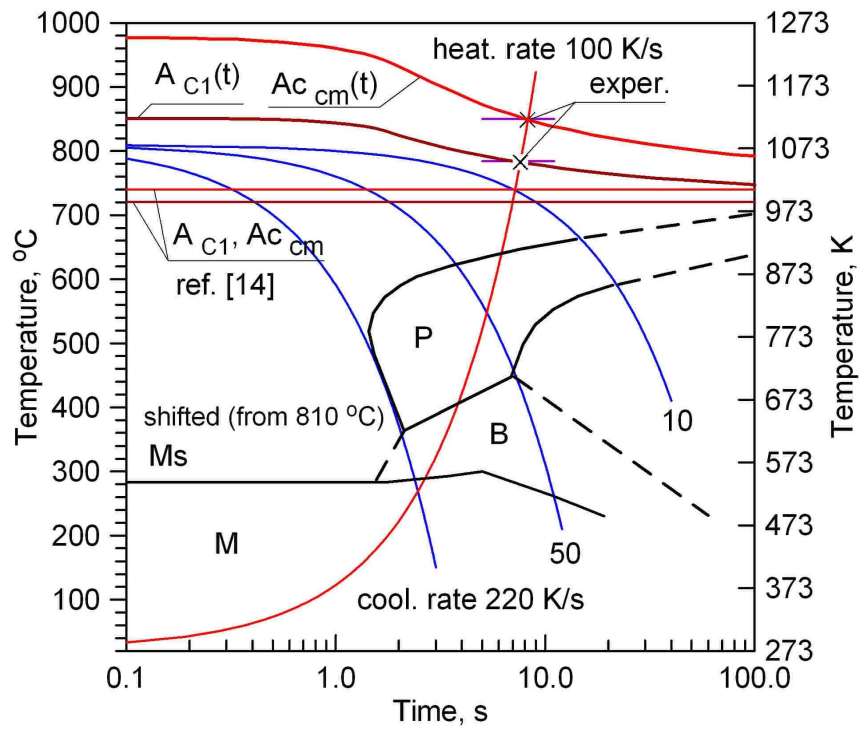Fig. 6. Diagram CCT for steel C80U [14]

Fig. 7. Shifted diagram CCT with CHT curves for considered steel [7]

After analysing of the above diagrams it can be noticed that steel under consideration does not contain ferrite but can contain remnant cementite [7] (Figs 5-7).

The curves of TTT or CCT diagrams are introduced into a relevant module of phase fraction determination with supplementary information regarding maximum participation of each phase $\left(\eta_{(\cdot)}^{\%}\right)$. However, in the model based upon the diagrams of continuous cooling relevant ranges determine the paces of cooling evaluated to the time when the temperature achieves the transformation starting curve whereas in the model based upon the isothermal diagrams the ranges of maximum phase participation are determined by times and temperatures at the beginning of the transformations.

In order to confirm the accuracy of the phase transformation model dilatometric tests were carried out on the samples of the steel under consideration. The tests were conducted at the Institute for Ferrous Metallurgy in Gliwice. The model was verified by comparing the dilatometric curves received for different cooling paces with simulation curves. On the basis of the analysis of the results a slight move of TTT and CCT diagrams was made in order to reconcile the initiation time of the simulation transformation and the times obtained in the experimental research (Fig. 7). These moves were presented, for example, in the studies [7].

On the basis of the analysis of simulation and dilatometric curves the values of the thermal expansion coefficient ($\alpha_{(\cdot)}$) and isotropic structural deformations of each structural component were specified. These coefficients are: 22, 10, 10 and 14.5 ($\times 10^{-6}$) [1/K] and 0.9, 4.0, 8.5 and 1.9 ($\times 10^{-3}$). It was adopted that 1,2,3,4 and 5 refer to austenite, bainite, martensite and pearlite, respectively [7]. In the steel grade under consideration no ferrite is present (η_3=0) and thus only four values were provided.

Exemplary comparisons of the simulation and experiment results are displayed in the figure 8. The transformation kinetics corresponding to the established speeds of cooling was presented in the Figure 9.
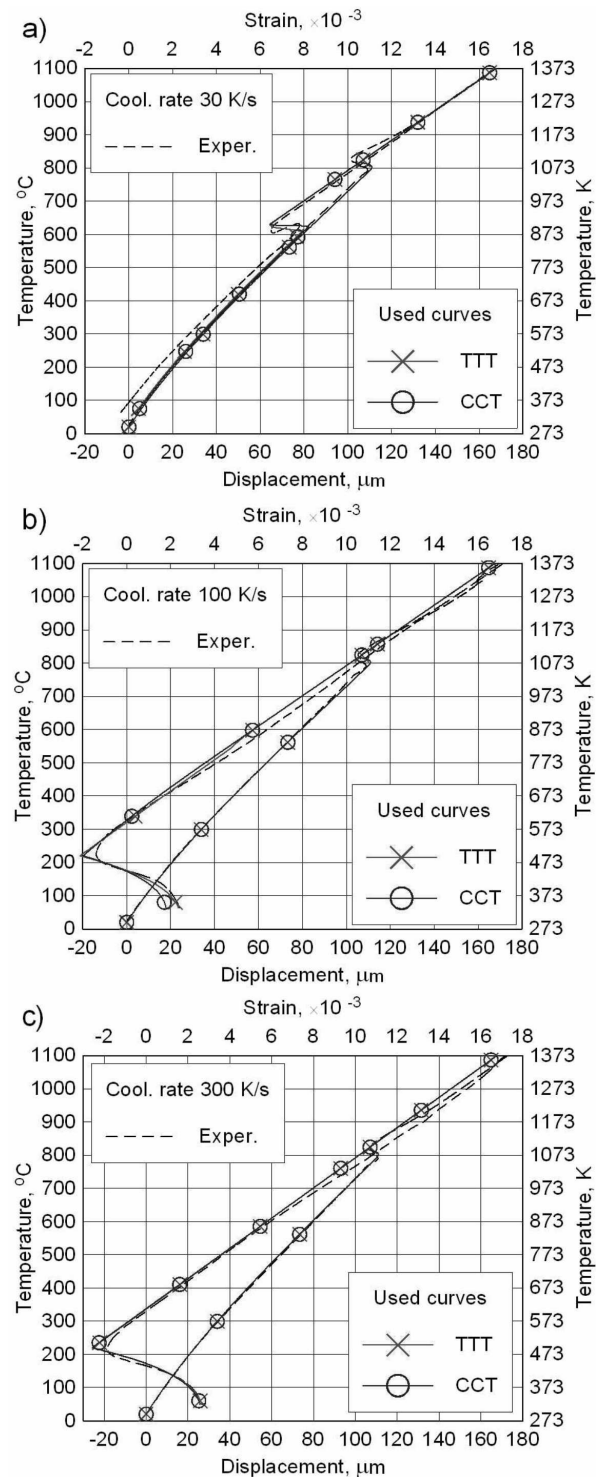

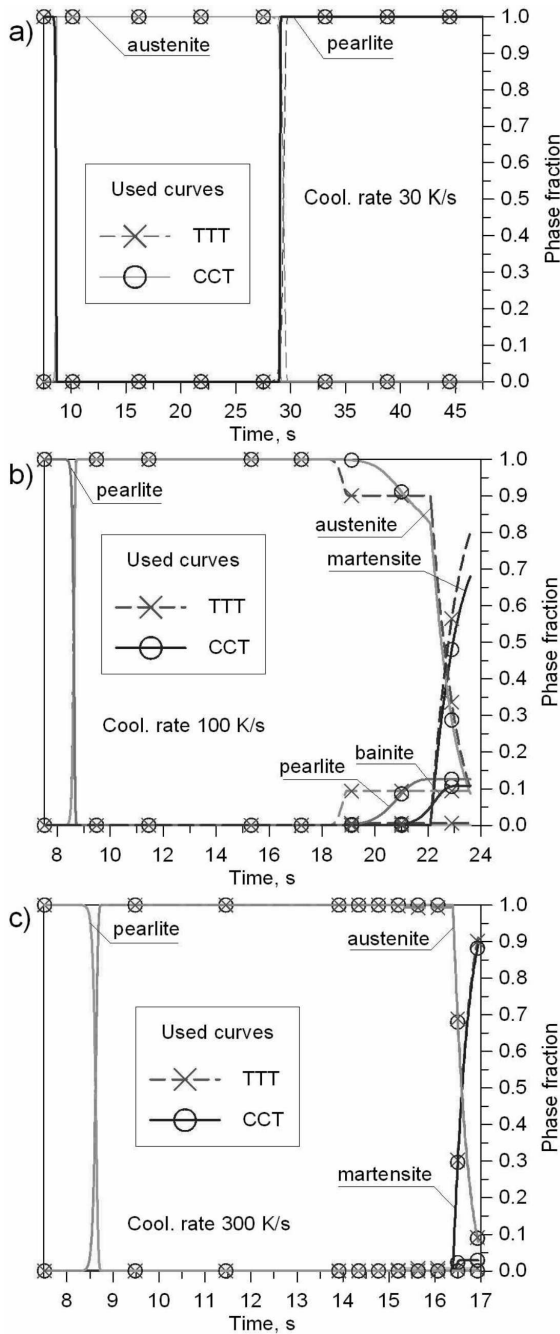Fig. 8. Experimental and simulating dilatometric curves

Fig. 9. Kinetics of phases for the fixed rates cooling

3. Temperature fields, stress and strain

Temperature field are obtain with solved of transient heat equation (Fourier equation) with source unit:

$$\nabla \cdot (\lambda \nabla (T)) - C \frac{\partial T}{\partial t} = -Q^v \tag{13}$$

where: $\lambda = \lambda(T)$ is the heat conductivity coefficient, $C = C(T)$ is effective heat coefficient, Q^v is intensity of internal source (this can also be the phase transformations heat).

Superficial heating investigation in model by boundary conditions Neumann (heat flux q_n), however cooling are modelling by boundary conditions Newton with depend on temperature coefficient of heat transfer:

$$-\lambda \frac{\partial T}{\partial n}\bigg|_\Gamma = q_n = \alpha^T (T)(T|_\Gamma - T_\infty) \tag{14}$$

In heating simulation on surfaces except heating source, also radiation through overall heat transfer coefficient was taken into account:

$$-\lambda \frac{\partial T}{\partial n}\bigg|_\Gamma = q_n = \alpha_0 \sqrt[3]{T|_\Gamma - T_\infty}(T|_\Gamma - T_\infty) = \alpha^* (T|_\Gamma - T_\infty) \tag{15}$$

where: α_0 is heat transfer coefficient experimental determine, Γ is surface, from witch is transfer heat, T_∞ is temperature of medium cooling.

Heat of phase transformations take into account in source unit of conductivity equation (13) calculate by formula:

$$Q^v = \sum_k H_k^{\eta_k} \dot{\eta}_k \tag{16}$$

where: $H_k^{\eta_k}$ is volumetric heat (enthalpy) k- phase transformations, $\dot{\eta}_k$ is rate of change fractions k- phase [2,20,21].

As it mention the problem solved by Finite Elements Method – in Galerkin formula [19].

In the model of mechanical phenomena the equations of equilibrium and constitutive relationship accept in rate form [2,9,19]:

$$\nabla \dot{\sigma} (x_\alpha, t) = \mathbf{0}, \quad \dot{\sigma} = \dot{\sigma}^T, \quad \dot{\sigma} = \mathbf{D} \circ \dot{\varepsilon}^e + \dot{\mathbf{D}} \circ \varepsilon^e \tag{17}$$

where: $\sigma = \sigma\left(\sigma^{\alpha\beta}\right)$ is stress tensor, $\mathbf{D} = \mathbf{D}(\nu, E)$ is tensor of material constant (isotropic material), ν is Poisson ratio, $E = E(T)$ is Young's modulus depend on temperature, whereas ε^e is tensor of elastic strain.

Make an assumption additive of strains, total strain in environment of considered point are results a sum:

$$\varepsilon = \varepsilon^e + \varepsilon^{Tph} + \varepsilon^{tp} + \varepsilon^p \tag{18}$$

where: ε^{Tph} are isotropic temperature and structural strain (see (10, 11)), ε^{tp} are transformations plasticity, whereas ε^p are plastic strain.

Coefficient of thermal expansion the pearlite structure for considered steel is dependent on temperature (Fig. 8), approximate this coefficient by square function [7].

$$\alpha_P = -1.2955 \cdot 10^{-11} T^2 + 2.5232 \cdot 10^{-8} T + \\ + 3.7193 \cdot 10^{-6} \; [1/K] \tag{12}$$

Analyse results from two-models notice, that advantageous is use in model of phase transformations the CCT graph for considered group steel. Accuracy results, particularly in range rate cooling are obtain, in witch forming also bainite (Fig. 9b).

To mark plastic strain the non-isothermal plastic law of flow with the isotropic strengthening and condition plasticity of Huber-Misses were used. Plasticize stress is depending on phase fraction, temperature and plastic strain

$$Y\left(T, \eta, \varepsilon_{ef}^p\right) = Y_0\left(T, \eta\right) + Y_H\left(T, \varepsilon_{ef}^p\right) \qquad (19)$$

where: $Y_0 = Y_0\left(T, \eta\right)$ is a yield points of material dependent on the temperature and phase fraction, $Y_H = Y_H\left(T, \varepsilon_{ef}^p\right)$ is a surplus of the stress resulting from the material hardening.

Transformations plasticity estimate are by Leblond formula, supplement of decrease function $(1-\eta_{(.)})$ propose by authors in work [17]:

$$\dot{\varepsilon}^{tp} = \begin{cases} 0, \eta_k \leqslant 0.03, \\ -3 \sum_{k=2}^{k=5} (1 - \eta_k)\, \varepsilon_{1k}^{ph} \frac{S}{Y_1} \ln(\eta_k)\, \dot{\eta}_k, \eta_k \geqslant 0.03 \end{cases} \qquad (20)$$

where: $3\varepsilon_{1k}^{ph}$ are volumetric structural strains when the material is transformed from the initial phase „1" into the k-phase, $\mathbf{S}$ is the deviator of stress tensor, Y_1 is plasticize stress of initial phase (austenite), beside

$$Y_1 = Y_1^0 + \kappa^{Y_1} \varepsilon_{ef}^{tp} \qquad (21)$$

Y_1^0 is yield points of initial phase nondeformation, $\kappa^{Y_1} = \kappa^{Y_1}(T)$ is hardening modulus of material on austenite structure, a ε_{ef}^{tp} is effective transformations strain. For reasons on lack suitable data was assumed, that $\kappa^{Y_1} = \kappa^Y(T)$.

Equation of equilibrium (17) solve by Finite Elements Method, and in range plasticization of material, iterative process modified method Newton-Raphson are perform [19].

4. Simulation example of hardening elements of machines

In the simulations of hardening was subject the fang lathe of cone (axisymmetrical object) made of tool steel. The shape and dimensions considered object was presented on the Figure 10.
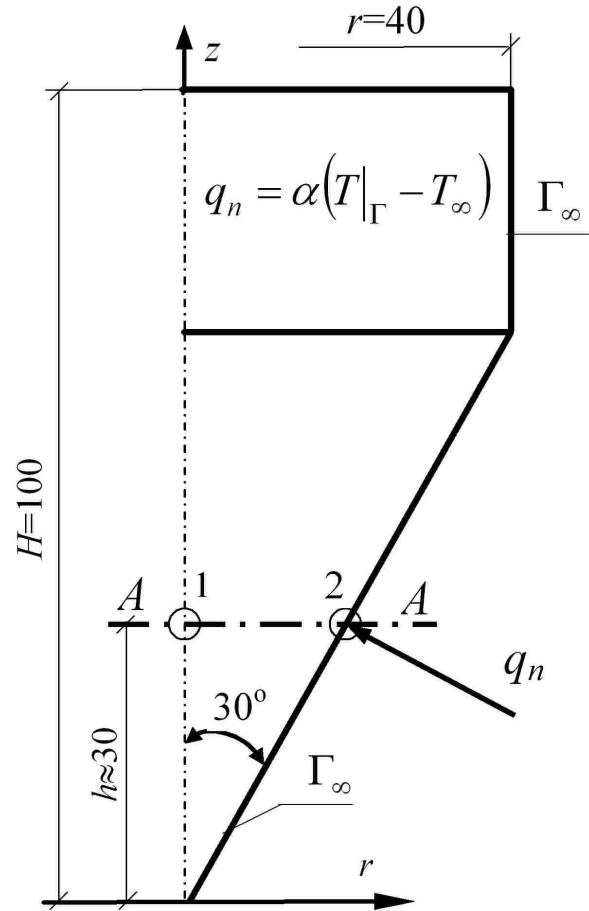

Fig. 10. Form and dimensions of the hardening object

The superficial heating (surface hardening) the section of side surface of cone was modelling Neumann boundary conditions taken Gauss distributions of heating source:

$$q_n = \frac{Q}{2\pi r^2} \exp\left(-\frac{(z-h)^2}{2r^2 \cos \alpha^2}\right) \qquad (22)$$

The peak value of heating source established on Q=3500 W, radius r=15 mm, angle α=30° (Fig. 10). The cooling of boundary contact with air was modelled boundary conditions (3.15) taking α_0=30 W/(m^{2}K) [4,9,22]. The initial structure was pearlite. The thermophysical values occurrence in conductivity equations (λ,C) was taken constant, averages values from passed in work data [4,5] suitable assumed: 35 [W/(mK)], 644*7760$\approx$5.0$\times$10^6 [J/(m^{3}K)]. The heat of phase transformations was determined on the work [4,20] assumed: H$_{AP}$=800$\times$10^6, H$_{AB}$=314$\times$10^6, H$_{AM}$=630$\times$10^6 [J/(m^{3}K)]. The initial temperature and ambient temperature was assumed equal 300 K.

In the modelling of mechanical phenomena the Young's and tangential modulus (E and E^t) was depend on temperature however the yield point (Y_0) on temperature and phase fractions. The values approximated of square functions (Fig. 11) assumed: Young's and tangential modulus 2.2×10^5 and 1.1×10^4 [MPa] ($E_t = 0.05E$), yield points 150, 400, 800 and 270 [MPa] suitably for austenite, bainite, martensite and pearlite, in temperature 300 K. In temperature 1700 K Young's and tangential modulus average 100 and 5 [MPa] siutable, however yield points are equal 5 [MPa].
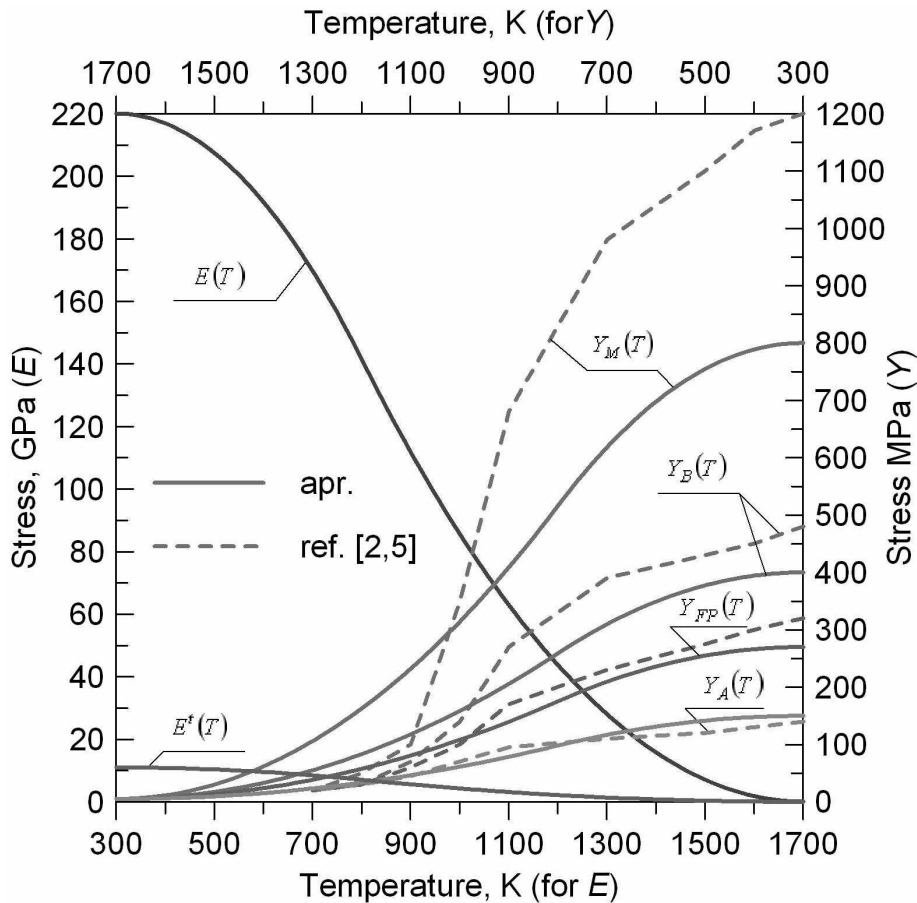
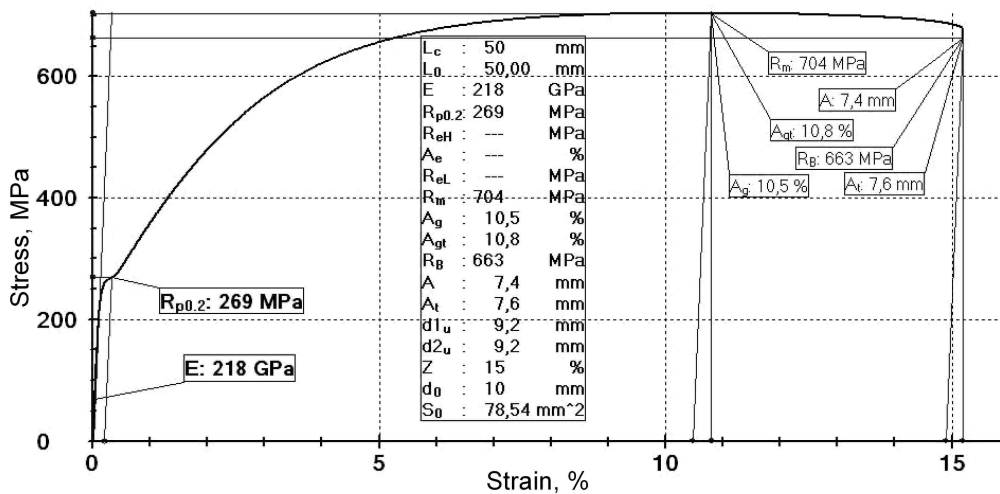Fig. 11. Diagrams of functions $E(T)$, $E^t(T)$ and $Y_0(T,\eta)$

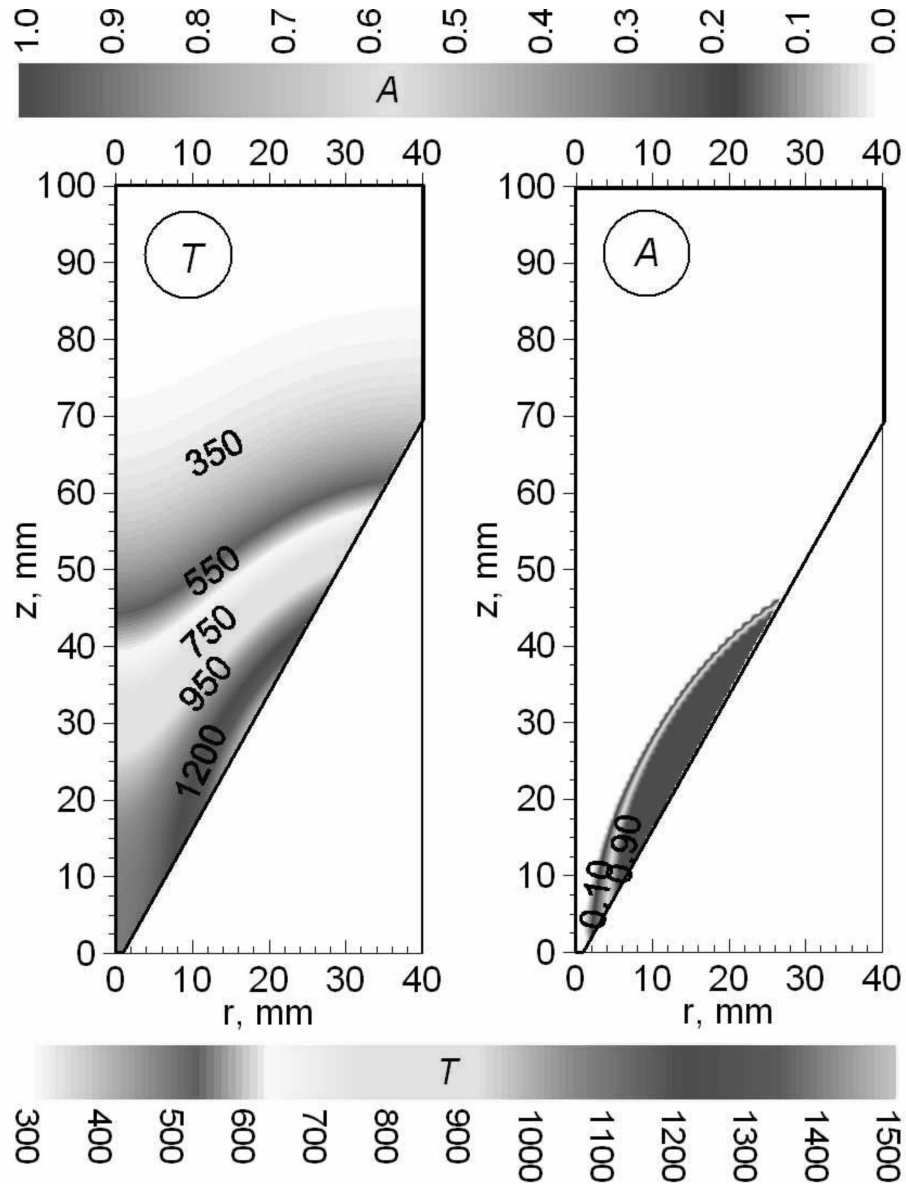Fig. 12. Curve of tension with designated characteristic values

Fig. 13. Distributions: temperature a) and austenite b) after heating

Young's and tangential modulus and yield point for pearlite in temperature 300 K establish on the basis own research estimated tension graph for considered steel (Fig. 12). The others values assumed on the literature [2,5,12]. Yield point for martensite assumed as average values presented through authors of works [2,4,5].

The heating performed to the moment of cross maximal temperature 1500 K in environment of heat source. Provide this obtain requirements austenite zone in parts conic fang lathe. The temperature distributions after heating and obtained zone of austenite presented on the Figure 13.

The cooling simulated by flux results from the difference of temperature among side surface and cooling medium (Newton condition). The temperature of cooling medium are equal 300 K. The coefficient of thermal conductivity was constant and was equal α^T=4000 [W/(m^{2}K)] (cooling in fluid layer [7,23]). The cooling performed to obtain by object ambient temperature, and final stress that residual stress. Obtained results of simulations were presented on following figures. The part of results along the radius (r) in cross section A-A and in distinguish points of cross sections (Fig. 10). This are the fields of external stress values, deposition of bainite and martensite.
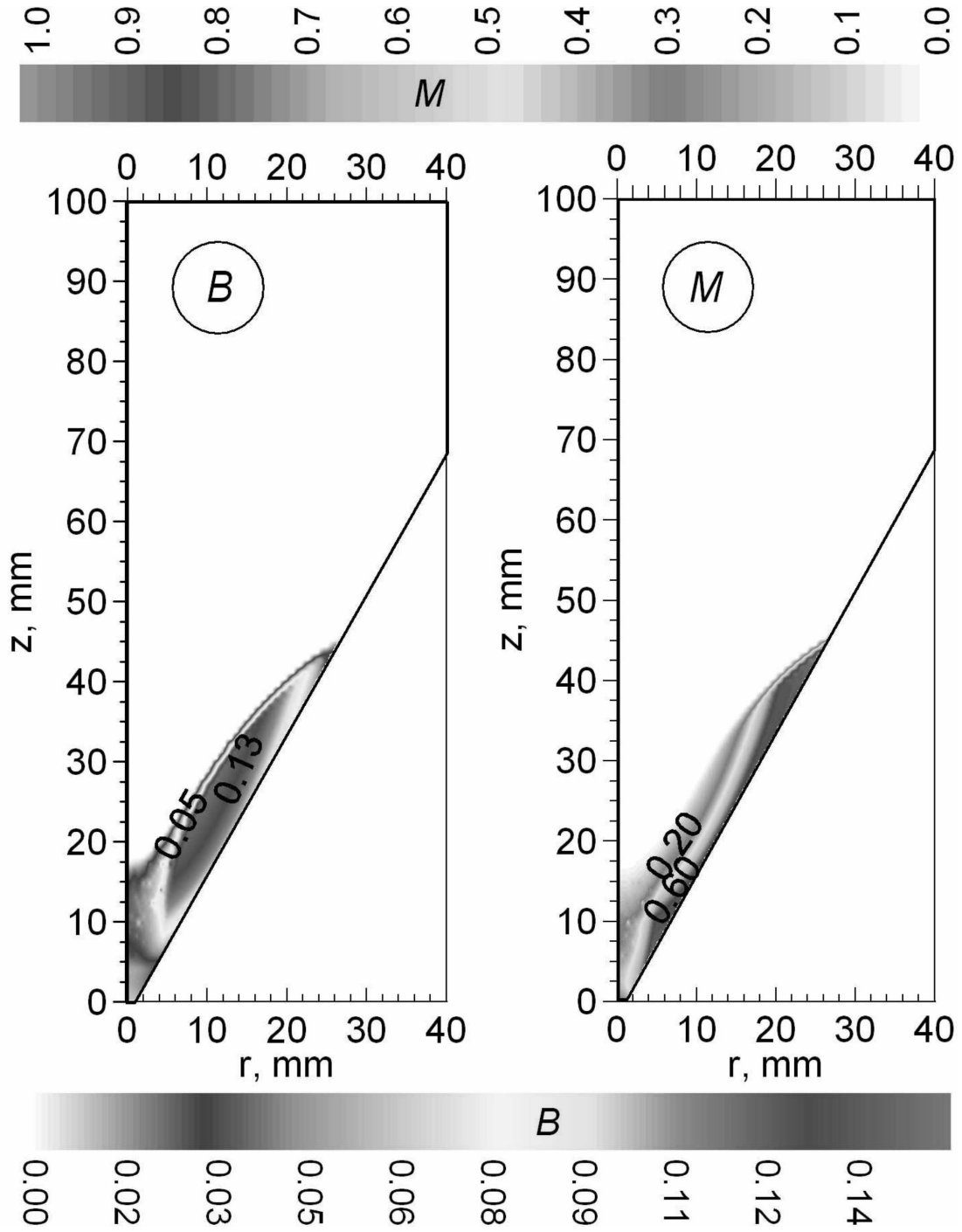
Fig. 14. Zones: bainite a) and martensite b) after quenching
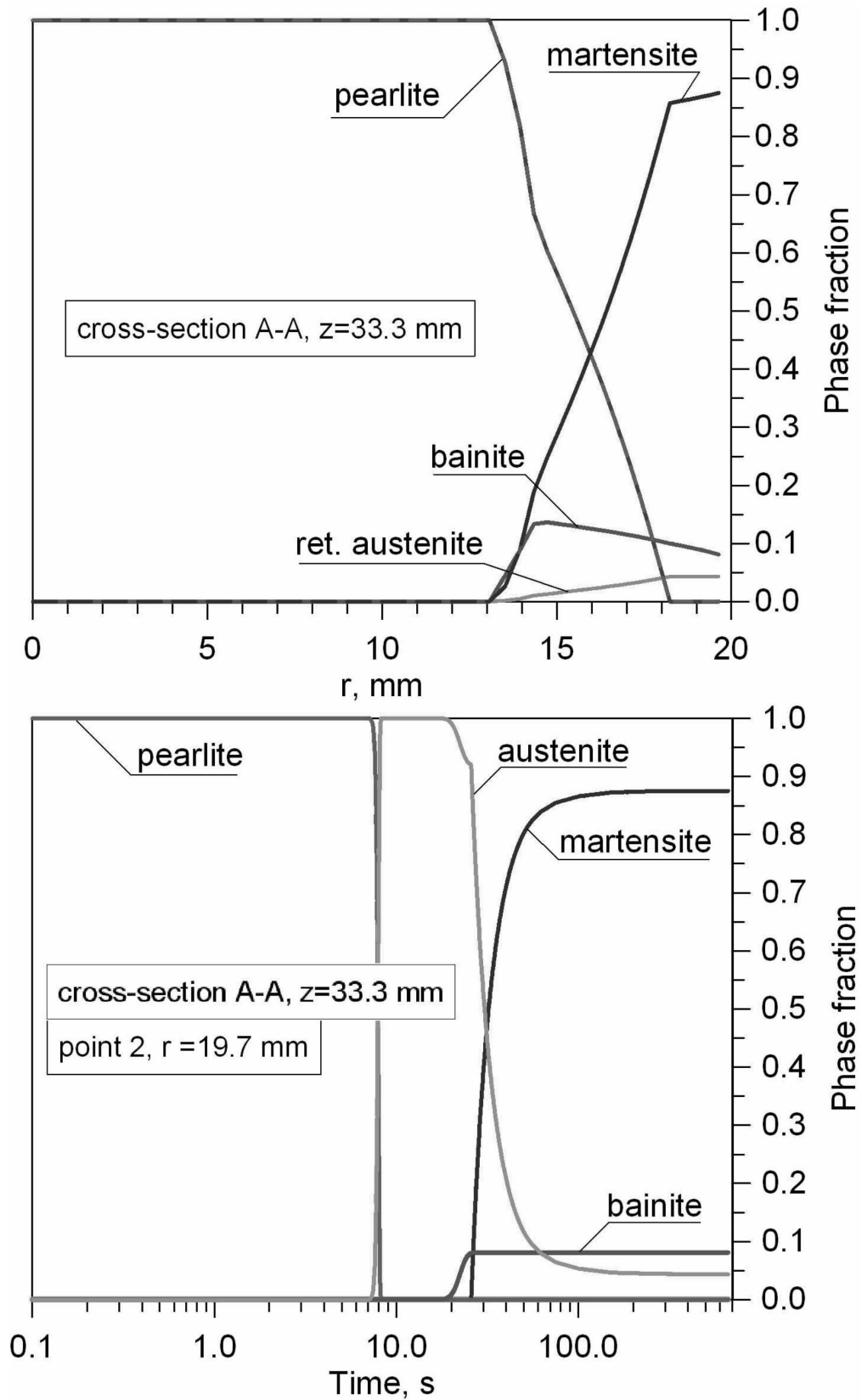
338

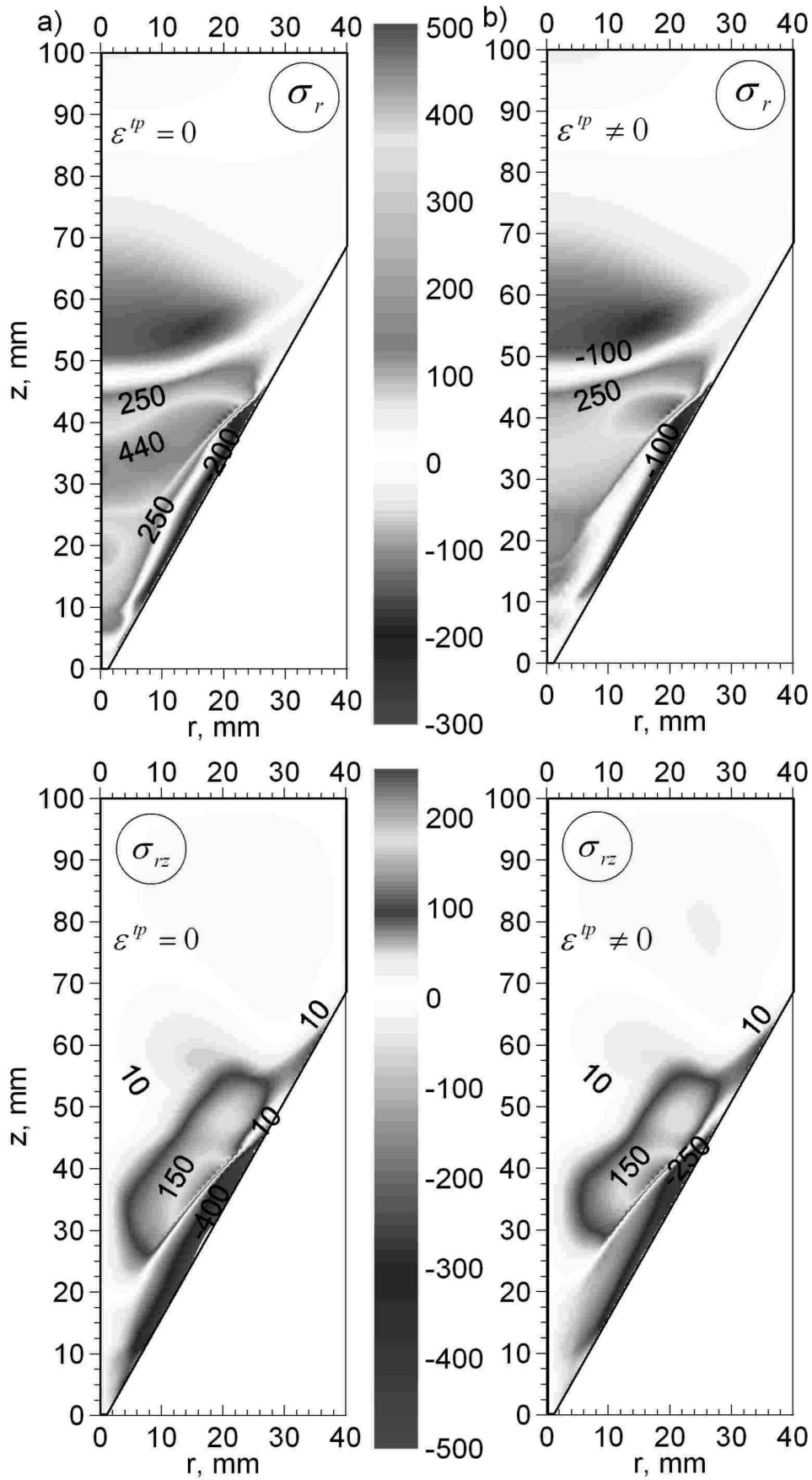Fig. 15. Phase fractions along radius (cross section A-A) and their kinetics in point 2 (Fig. 10)

Fig. 16. Distributions of radial and tangential stresses: without a) and with b) transformations plasticity
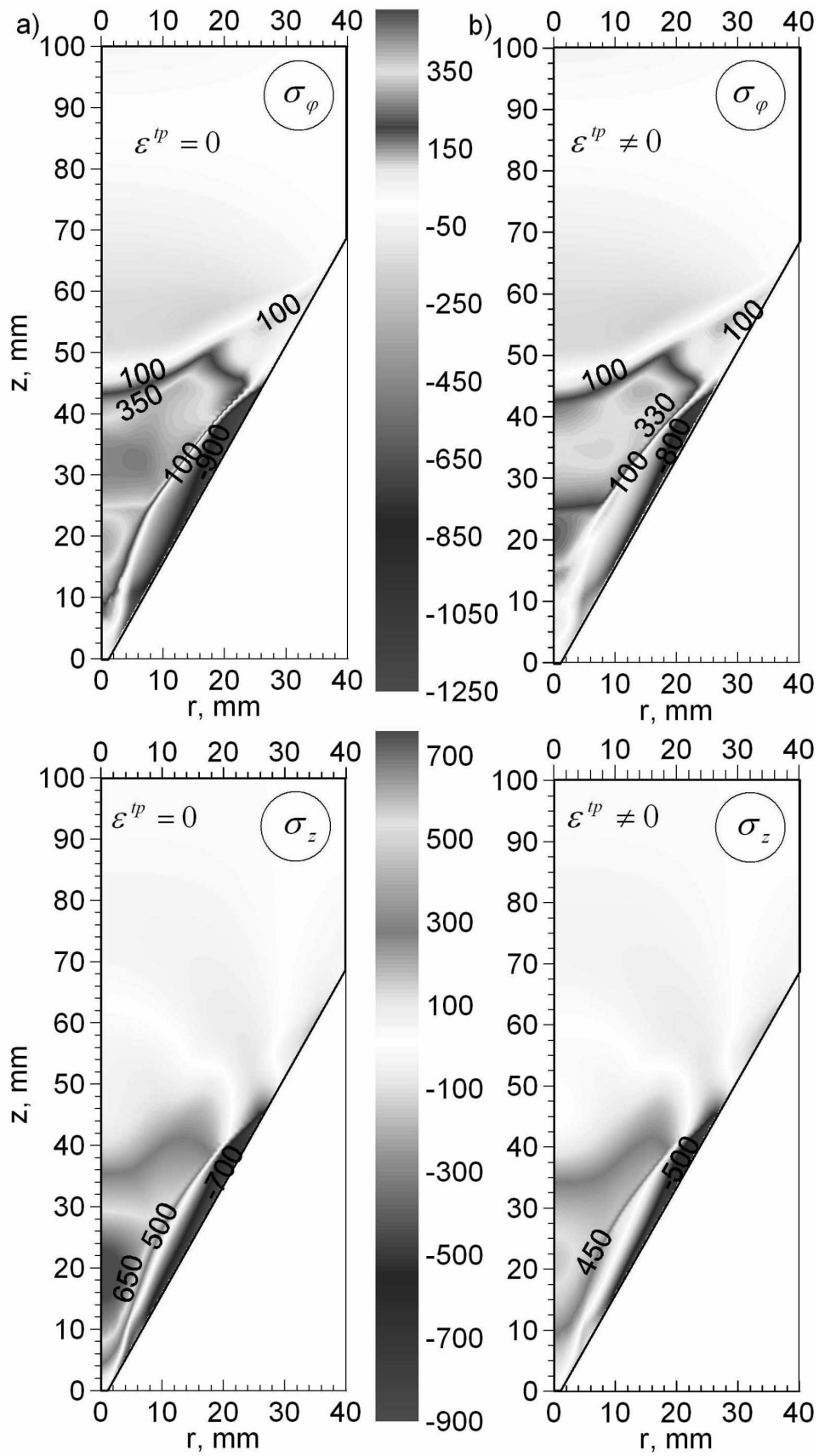
Fig. 17. Distributions of circumferential and axial stresses: without a) and with b) transformations plasticity
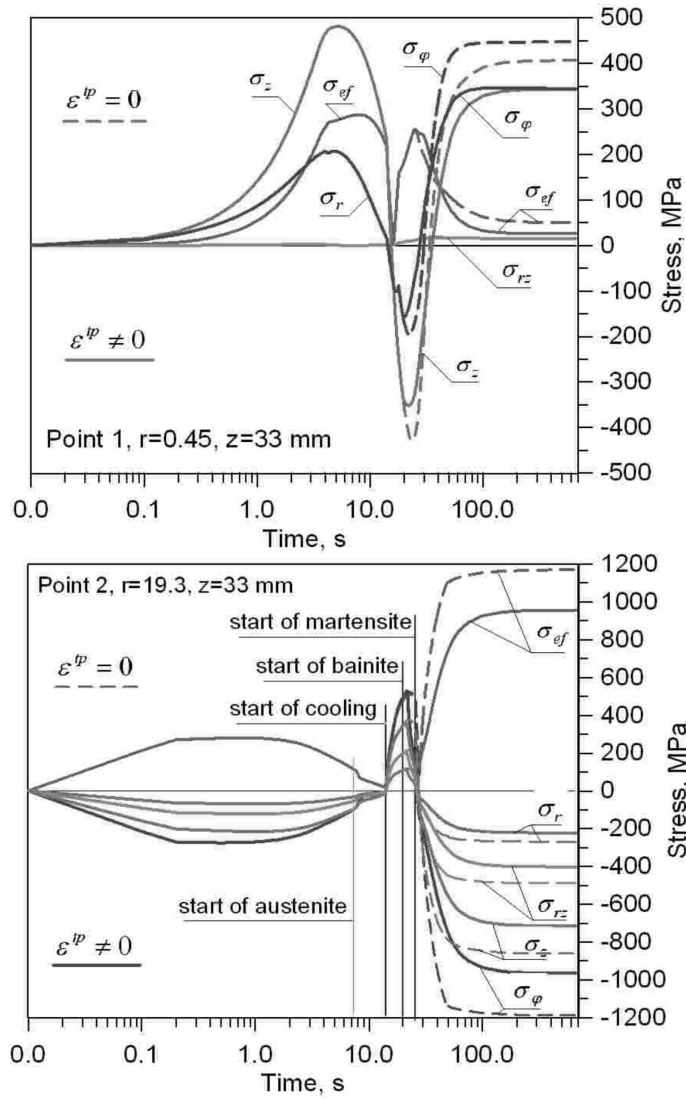
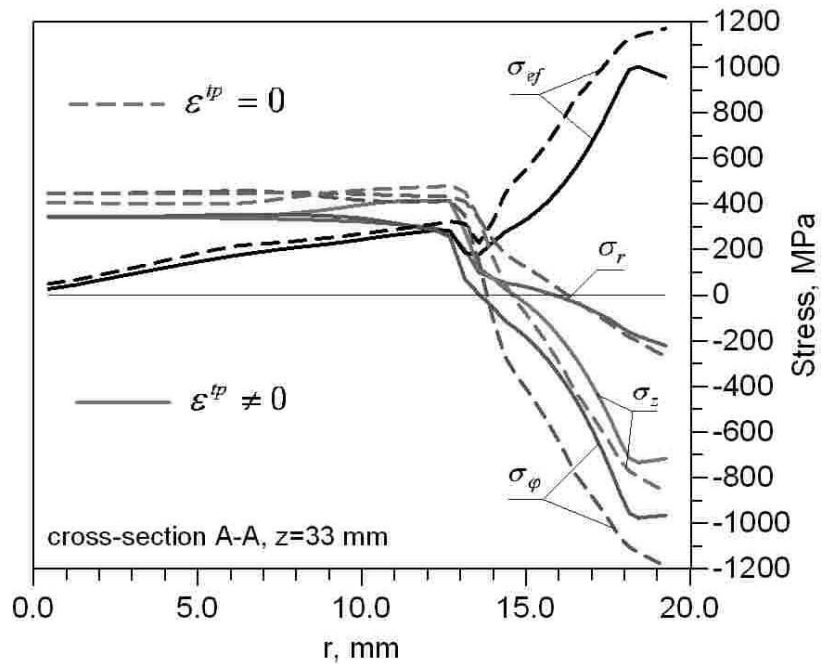Fig. 18. History of temporary stresses in distinguished points of the cross section A-A

Fig. 19. Distributions of residual stresses along radius (cross section A-A)
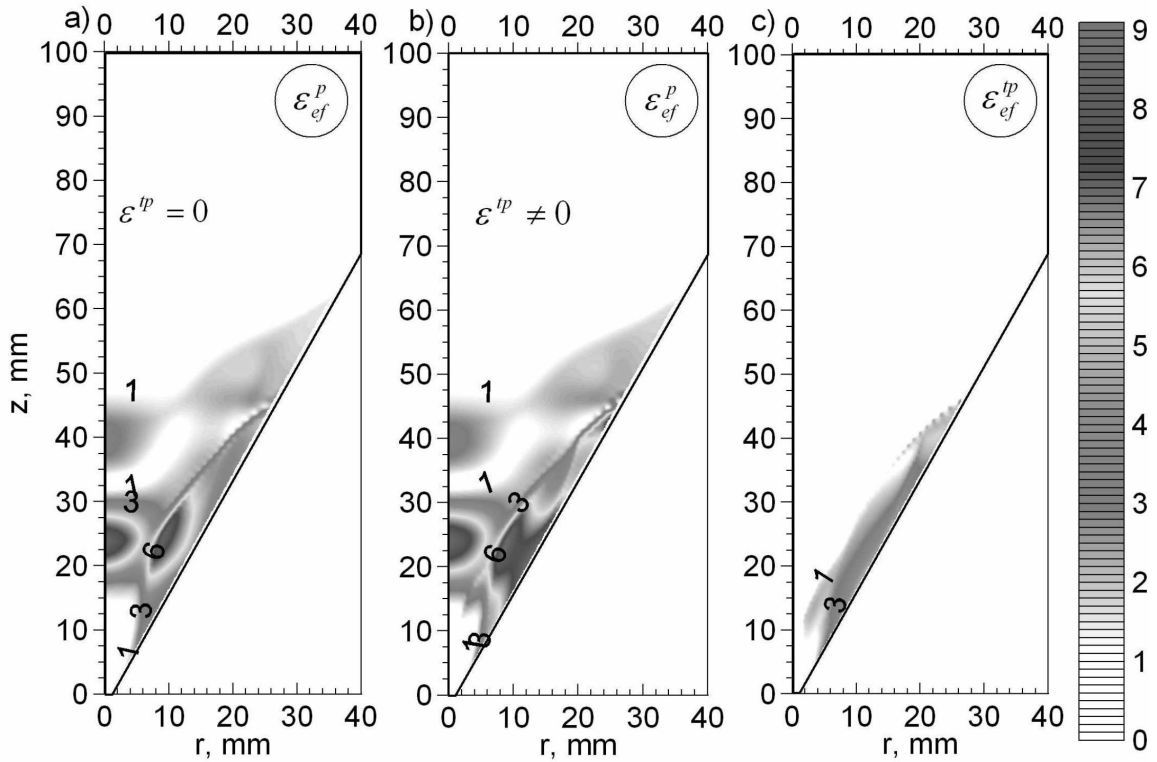
Fig. 20. Distributions of effective plastic strains and transformations plasticity ($\times 10^3$): without a) and with b) transformations plasticity, c) transformations plasticity
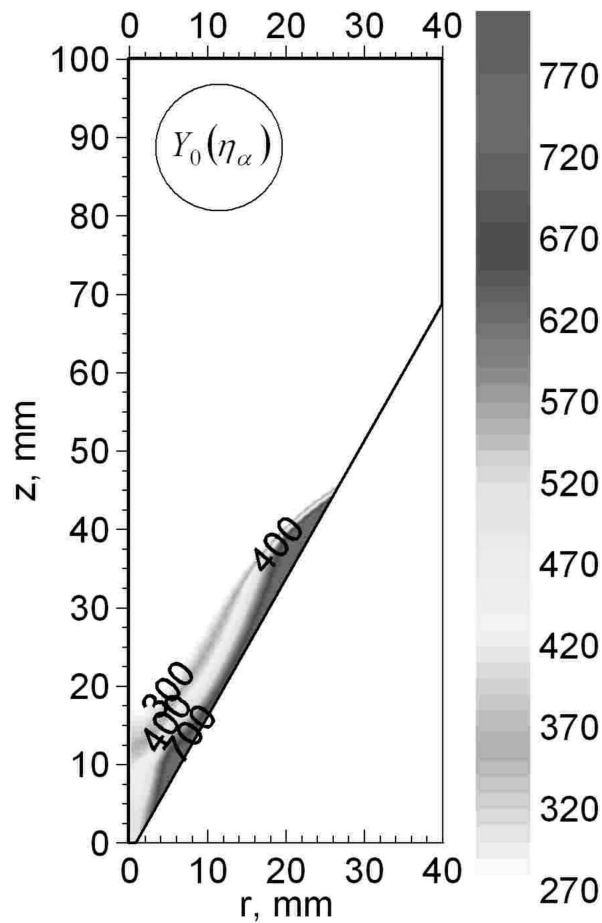

Fig. 21. Distributions of the yield point after quenching

5. Summary and conclusions

As it has been already mentioned, using of TTT diagrams in numerical models for determination of newly-created phase fractions enables parallel calculations and it is easier to include phase transformation heat in the numerical algorithm. However, using CCT diagrams within the cooling rate ranges wherein three transformations are observed: pearlitic, bainitic and martenisitic, guarantees more precise results. The examples are shown in figures 8 and 9. The results obtained with the application of CCT diagram are closer to the results of experimental research. The results of simulation of phase fractions obtained after application of TTT or CCT diagrams for small and high rates of cooling are highly comparable (Figs 8a,8c and 9a,9c). It is optimistic, however, that for medium rates of cooling (100 K/s, Figs 8b,9b) a little bit more martensite is received at the expense of bainite meaning that a comparable hardened zone is obtained. It was confirmed that mechanical phenomena simulation results are comparable in both models. Nevertheless, the results of verification simulation of phase transformation kinetics (Figs 8b and 9b) prove that application of CCT diagrams enables more precise determination of fractions and kinetics of newly-created phases depending on the cooling rate. Therefore for simulating phase transformations in the object undergoing hardening of the calculation example (fang lathe) a model based upon CCT diagrams was used (Fig. 7).

The selected method of heating of the fang lathe undergoing hardening is very beneficial. A very valuable distribution of temperature and good area of austenite deposition were obtained (Fig. 13). The hardened area after cooling appeared very beneficial, as well, which means that it is very well situated. The structure of the area after hardening is very good (certain fraction of bainite and significant fraction of martensite) (Figs 14 and 15). In the hardened zone a small fraction of retained austenite (approximately 5%) was received, too (Fig. 15). The point of the lathe was not hardened at all. It is very valuable from the practical point of view with respect to the purpose of such a machinery part.

Distribution of stresses after such hardening is beneficial, as well. Accumulation of stresses is observed only in the zone undergoing hardening and normal stresses are negative in the subsurface layer (Figs 16-19). There are almost no stresses in the lathe core and point (see Figs 16,17). Influence of transformation plasticity is noticeable (see Figs 16-18) but is insignificant since it is subsurface hardening. However, taking into account structural strain is very significant for mechanical phenomena. It is presented in the figure displaying the history of

instantaneous stresses in the distinguished points of the section A-A (Fig. 18). The plastic strain zone is beneficial since it was created in the working part of the lat he. Yet, plastic and transformation strain are not high (Fig. 20). Increased yield point received in the hardened zone (working part of the lathe) is also valuable (Fig. 21). It indicates increased hardness of the subsurface layers of this part of the heavy duty fang lathe undergoing hardening.

REFERENCES

[1] S-H. K a n g, Y.T. I m, Finite element investigation of multi-phase transformation within carburized carbon steel. Journal of Materials Processing Technology **183**, 241-248 (2007).

[2] S-H. K a n g, Y.T. I m, Three-dimensional thermo-elestic-plastic finite element modeling of quenching process of plain carbon steel in couole with phase transformation. Journal of Materials Processing Technology **192-193**, 381-390 (2007).

[3] A. B o k o t a, A. K u l a w i k, Model and numerical analysis of hardening process phenomena for medium-carbon steel, Archives of Metallurgy and Materials **52**, 2, 337-346 (2007).

[4] W.P O l i v e i r a, M.A. S a v i, P.M.C.L. P a c h e c o, L.F.G. S o u z a, Thermomechanical analysis of steel cylinders with diffusional and non-diffusional phase transformations. Mechanics of Materials **42**, 31-43 (2010).

[5] M. C o r e t, A. C o m b e s c u r e, A mesomodel for the numerical simulation of the multiphasic behavior of materials under anisothermal loading (application to two low-carbon steels), International Journal of Mechanical Sciences **44**, 1947-1963 (2002).

[6] S.H. K a n g, Y.T. I m, Thermo-elesto-plastic finite element analysis of quenching process of carbon steel. International Journal of Mechanical Sciences **49**, 13-16 (2007).

[7] A. B o k o t a, T. D o m a ń s k i, Numerical analysis of thermo-mechanical phenomena of hardening process of elements made of carbon steel C80U, Archives of Metallurgy and Materials **52**, 2, 277-288 (2007).

[8] P. U l i a s z, T. K n y c h, A. M a m a l a, A new industrial-scale method of the manufacturing of the gradient structure materials and its application. Archives of Metallurgy and Materials **54**, 3, 711-721 (2009).

[9] B. R a n i e c k i, A. B o k o t a, S. I s k i e r k a, R. P a r k i t n y, Problem of Determination of Transient and Residual Stresses in a Cylinder under Progressive Induction Hardening. Proceedings of 3rd International Conference On Quenching And Control Of Distortion. Published by ASM International, 473-484 (1999).

[10] E.P. S i l v a, P.M.C.L. P a c h e c o, M.A. S a v i, On the thermo-mechanical coupling in austenite-martensite phase transformation related to the quenching process,

International Journal of Solids and Structures **41**, 1139-1155 (2004).

[11] D.Y. J u, W.M. Z h a n g, Y. Z h a n g, Modeling and experimental verification of martensitic transformation plastic behavior in carbon steel for quenching process, Material Science and Engineering **A 438-440**, 246-250 (2006).

[12] M. C o r e t, S. C a l l o c h, A. C o m b e s c u r e, Experimental study of the phase transformation plasticity of 16MND5 low carbon steel induced by proportional and nonproportional biaxial loading paths. European Journal of Mechanics A/Solids **23**, 823-842 (2004).

[13] M. P i e t r z y k, Through-process modelling of microstructure evolution in hot forming of steels, Journal of Materials Technology **125-126**, 53-62 (2002).

[14] M. B i a ł e c k i, Characteristic of steels, series F, tom I, Silesia Editor, (1987) 108-129, 155-179, (in polish).

[15] M. S u l i g a, Z. M u s k a l s k i, The influence of single draft on TRIP effect and mechanical propertiesof 0.09C-1.57Mn-0.9Si steel wires. Archives of Metallurgy and Materials **54**, 3, 677-684 (2009).

[16] M. C h e r k a o u i, M. B e r v e i l l e r, H. S a b a r, Micromechanical modeling of martensitic transformation induced plasticity (TRIP) in austenitic single crystals, International Journal of Plasticity **14**, 7, 597-626 (1998).

[17] L. T a l e b, F. S i d o r o f f, A micromechanical mod-

elling of the Greenwood-Johnson mechanism in transformation induced plasticity, International Journal of Plasticity **19**, 1821-1842 (2003).

[18] S. S e r e j z a d e h, Modeling of temperature history and phase transformation during cooling of steel, Journal of Processing Technology **146**, 311-317 (2004).

[19] O.C. Z i e n k i e w i c z, R.L. T a y l o r, The finite element method, Butterworth-Heinemann, Fifth edition **1**, 2 (2000).

[20] K.J. L e e, Characteristics of heat generation during transformation in carbon steel. Scripta Materialia **40**, 735-742 (1999).

[21] L. H u i p i n g, Z. G u o q u n, N. S h a n t i n g, H. C h u a n z h e n, FEM simulation of quenching process and experimental verification of simulation results, Material Science and Engineering **A 452-453**, 705-714 (2007).

[22] A. B o k o t a, S. I s k i e r k a, Numerical analysis of phase transformation and residual stresses in steel cone-shaped elements hardened by induction and flame methods. International Journal of Mechanical Sciences **40** (6), 617-629 (1998).

[23] J. J a s i ń s k i, Influence of fluidized bed on diffusional processes of saturation of steel surface layer. Seria: Inżynieria Materiałowa Nr 6, Editor WIPMiFS, Częstochowa (2003), (in polish).